

Enhancement of the Photovoltaic Performance of $\text{CH}_3\text{NH}_3\text{PbI}_3$ Perovskite Solar Cells through a Dichlorobenzene-Functionalized Hole-Transporting Material

Jin-Wook Lee,^[a] Sungmin Park,^[b, c] Min Jae Ko,^[b] Hae Jung Son,^{*,[b]} and Nam-Gyu Park^{*,[a]}

A dichlorobenzene-functionalized hole-transporting material (HTM) is developed for a $\text{CH}_3\text{NH}_3\text{PbI}_3$ -based perovskite solar cell. Notwithstanding the similarity of the frontier molecular orbital energy levels, optical properties, and hole mobility between the functionalized HTM [a polymer composed of 2'-butyloctyl-4,6-dibromo-3-fluorothieno[3,4-*b*]thiophene-2-carboxylate (TT-BO), 3',4'-dichlorobenzyl-4,6-dibromo-3-fluorothieno[3,4-*b*]thiophene-2-carboxylate (TT-DCB), and 2,6-bis(trimethyltin)-4,8-bis(2-ethylhexyloxy)benzo[1,2-*b*:4,5-*b'*]dithiophene (BDT-EH), denoted PTB-DCB21] and the nonfunctionalized polymer [a polymer composed of thieno[3,4-*b*]thiophene (TT) and benzo[1,2-*b*:4,5-*b'*]dithiophene (BDT), denoted PTB-BO],

a higher power conversion efficiency for PTB-DCB21 (8.7%) than that for PTB-BO (7.4%) is achieved because of a higher photocurrent and voltage. The high efficiency is even obtained without including additives, such as lithium bis(trifluoromethanesulfonyl)imide and/or 4-*tert*-butylpyridine, that are commonly used to improve the conductivity of the HTM. Transient photocurrent–voltage studies show that the PTB-DCB21-based device exhibits faster electron transport and slower charge recombination; this might be related to better interfacial contact through intermolecular chemical interactions between the perovskite and the 3,4-dichlorobenzyl group in PTB-DCB21.

1. Introduction

Since the first report on the high efficiency of an all-solid-state sensitized thin-film solar cell based on a perovskite $\text{CH}_3\text{NH}_3\text{PbI}_3$ light harvester,^[1] organolead halide perovskite-based solar cells have received much attention due to facile fabrication, superb photovoltaic performance, and “dirt cheap” solar power technology. Due to excellent optoelectrical properties of the organolead halide perovskite, a power conversion efficiency (PCE) of 15% was demonstrated.^[2,3] Organometal halide perovskite has the general formula of RMX_3 (R = monovalent organic cation, M = divalent metal cation and X = halogen), in which R is a cation coordinated with twelve X anions and M is a cation with six X anions, resulting in a cubo-octahedron and an octahedron, respectively. Layered tin-based perovskite materials have interesting physical properties, such as semiconductor-to-


metal transition^[4] and light-emitting^[5] properties. Unlike intensive studies on tin-based halide perovskite, lead-based halide perovskite has less attracted attention because of undesirable optoelectronic properties for superconductor or light-emitting display applications. $\text{CH}_3\text{NH}_3\text{PbX}_3$ ($\text{X} = \text{Br}, \text{I}$) was first applied to electrochemical junction solar cells comprising porous TiO_2 as an alternative to binary quantum dots, which showed PCEs of 3–4%.^[6] A significant improvement in efficiency was achieved by optimizing the concentration of the perovskite coating solution, the thickness of the perovskite-coated TiO_2 layer, and the electrolyte formulation; this resulted in a PCE of 6.5%.^[7] However, these devices suffered from low stability because the perovskite was easily degraded by liquid electrolytes. A breakthrough in the device performance and stability was made by replacing the liquid electrolyte with a solid-state hole-transporting material (HTM), such as 2,2',7,7'-tetrakis(*N,N*-p-dimethoxyphenylamino)-9,9'-spirobifluorene (spiro-MeOTAD). An all-solid-state solar cell based on the junction between the $\text{CH}_3\text{NH}_3\text{PbI}_3$ nanocrystals adsorbed on a 0.6 μm thick TiO_2 film and spiro-MeOTAD demonstrated a PCE of 9.7%.^[11] and the device with a mesoporous Al_2O_3 film decorated with the mixed halide perovskite $\text{CH}_3\text{NH}_3\text{PbI}_2\text{Cl}$ instead of the TiO_2 layer showed a PCE of 10.9%.^[8] It was argued that the perovskite layer acted as a charge transporter for the case of Al_2O_3 , which might have been associated with the charge accumulation ability of the perovskite light harvester.^[9] Recently, a remarkable improvement in PCE of around 15% was achieved by either a mesoscopic structure^[2] or a flat p–n junction structure.^[3]

[a] J.-W. Lee,⁺ Prof. N.-G. Park
School of Chemical Engineering and Department of Energy Science
Sungkyunkwan University, Suwon, 440-746 (Korea)
Fax: (+82) 31-290-7241
E-mail: npark@skku.edu

[b] S. Park,⁺ Dr. M. J. Ko, Dr. H. J. Son
Photoelectronic Hybrid Research Center
Korea Institute of Science and Technology, Seoul 136-791 (Korea)
Fax: (+82) 2-958-6649
E-mail: hjson@kist.re.kr

[c] S. Park⁺
Department of Chemistry, Korea University, Seoul 136-713, (Korea)

⁺ These authors contributed equally to this work.

 Supporting Information for this article is available on the WWW under <http://dx.doi.org/10.1002/cphc.201402033>.

Apart from a small-molecule HTM, such as spiro-MeOTAD, polymer-based HTMs have been developed. Compared with small molecules, the polymers have important advantages as a HTM in terms of processability, thermomechanical stability, and charge transport.^[10–13] However, although perovskite-based solar cells employing polymer HTMs recently showed good performances with a high PCE of up to 12%,^[14] only a few polymers, such as poly(3-hexylthiophene) (P3HT) and polytriarylamine (PTAA), have been demonstrated as effective HTMs.^[15,16] To obtain high photovoltaic performance, it is important to develop new hole-transporting polymers and gain a deeper understanding of the relationship between solar cell properties and the polymer's structure. Therefore, to address these issues, we have directed our attention toward the synthesis of new hole-transporting polymers with the following points in mind:^[17–23] 1) high hole mobility, 2) optimal HOMO energy level to maximize an open-circuit voltage to provide a driving force enough for effective hole transport from the perovskite to the polymer in the solar cell device, 3) good solubility for device fabrication, and 4) complete penetration of the polymer into the pores of the mesoporous TiO₂ electrodes. More importantly, the formation of a good junction at the interface of the perovskite and polymer is needed for effective hole transfer from the perovskite to the polymer and minimizing charge recombination loss. Therefore, we have been interested in improving the junction between the perovskite and the polymer by increasing their intermolecular chemical interactions. For this, we designed a new polymer, in which conventional solubilizing groups, hydrophobic alkyl side chains, attached on the conductive polymer backbone were partially replaced by 3,4-dichlorobenzyl groups because the hydrophilic perovskite might have been able to make better intermolecular interactions with the 3,4-dichlorobenzyl groups rather than the alkyl chains through intermolecular chemical interactions, such as ion–dipole and cation– π interactions. The polymer backbone was composed of two repeating units of thieno[3,4-*b*]thiophene (TT) and benzo[1,2-*b*:4,5-*b'*]dithiophene (BDT), resulting in a TT-BDT alternating copolymer because they are effective for increasing polymer's hole mobility by endowing a polymer backbone planarity and thereby, π – π intermolecular interactions.^[24–26]

In the paper, we report on the synthesis of TT-BDT alternating copolymers with and without a 3,4-dichlorobenzyl group and the effect of functionalization of the polymer on photovoltaic performance of the CH₃NH₃PbI₃-based perovskite solar cell employing the polymer as a HTM, along with long-term device stability. A higher PCE of 8.7% was demonstrated from the HTM polymer with the 3,4-dichlorobenzyl group than that without the functional group (PCE = 7.4%). Transient photocurrent and voltage spectroscopic studies were performed for understanding the basis for the improved photovoltaic performance of the perovskite solar cell device when using the 3,4-dichlorobenzyl group functionalized polymer as a HTM.

2. Results and Discussion

Scheme 1 represents the synthetic route of the polymer prepared from 2'-butyloctyl-4,6-dibromo-3-fluorothieno[3,4-*b*]thiophene-2-carboxylate (TT-BO), 3',4'-dichlorobenzyl-4,6-dibromo-3-fluorothieno[3,4-*b*]thiophene-2-carboxylate (TT-DCB), and 2,6-bis(trimethyltin)-4,8-bis(2-ethylhexyloxy)benzo[1,2-*b*:4,5-*b'*]dithiophene (BDT-EH), denoted herein as PTB-DCB21. Each monomer was obtained according to modified literature procedures^[27] and the polymerization was performed with a feed ratio of *m/n* (molar ratio) = 0.79:0.21 through Stille coupling polymerization. Due to the solubility issue of the polymer, we did not increase the feed ratio of TT-DCB more than 0.21 for the polymerization.^[28] For comparison, an alternating copolymer of TT and BDT (PTB-BO) was also prepared. The resulting polymers were soluble in chlorinated solvents, such as chloroform, chlorobenzene, and *o*-dichlorobenzene, and the molecular weights (*M_n*) estimated by gel-permeation chromatography (GPC) at room temperature were *M_n* = 104.9 and 112.0 kg mol^{−1} with polydispersity indices (PDI) of 5.48 and 2.77 for PTB-DCB21 and PTB-BO, respectively. Thermogravimetric analysis (TGA) shows that PTB-BO is more stable than PTB-DCB21, but both polymers are stable up to >250 °C (Figure S1 in the Supporting Information). For both polymers, no clear glass transition is observed from 30 to 270 °C in the differential scanning calorimetry (DSC) curves of the second heating and cooling runs (10 °C min^{−1}; Figure S2 in the Supporting Information).

The UV/Vis absorption spectra of PTB-DCB21 and PTB-BO in a film are shown in Figure 1. The polymers show very similar

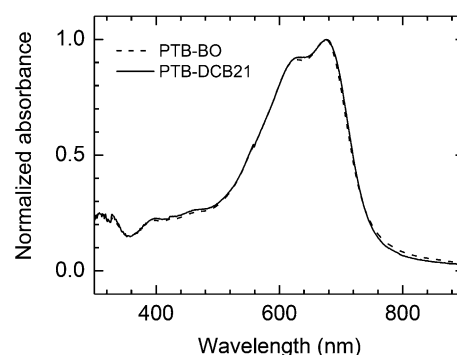
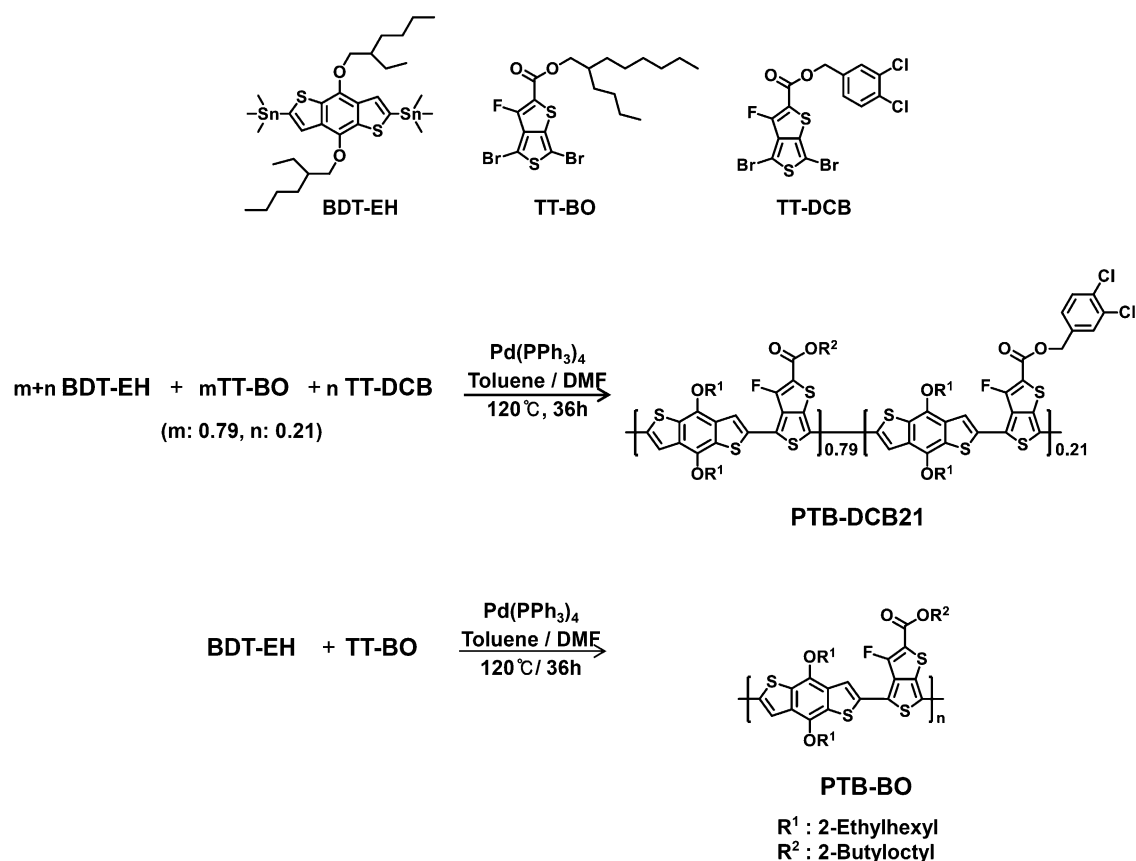


Figure 1. UV/Vis absorption spectra of PTB-BO (dashed line) and PTB-DCB21 (solid line) in a film.

absorption features to each other with maxima at about $\lambda = 675$ nm; this suggests that incorporation of the 3,4-dichlorobenzyl group as a side chain of the polymer does not induce any significant change in the ordered molecular structure of the polymer in the thin film. From the onset of the absorption spectra, optical band gaps are estimated to be about 1.66 eV for both polymers.

The electrochemical properties of PTB-DCB21 and PTB-BO have been investigated by using cyclic voltammetry (CV) and the polymers exhibit quasi-reversible oxidation/re-reduction processes in the positive potential range and reversible reduc-



Scheme 1. Synthetic routes for polymers PTB-DCB21 and PTB-BO. DMF = *N,N*-dimethylformamide.

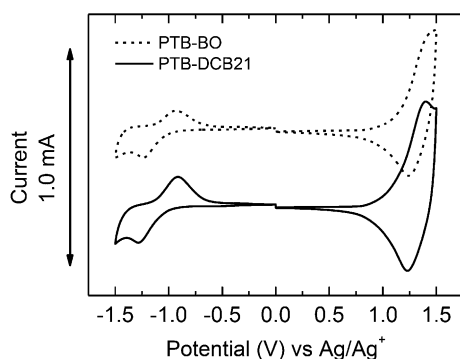


Figure 2. Cyclic voltammograms of PTB-BO (dashed line) and PTB-DCB21 (solid line).

tion/re-oxidation processes in the negative potential range; this indicates good electrochemical stability of the polymers (Figure 2). The LUMO and HOMO energy levels of the polymers are determined from the onset redox potentials. Compared with PTB-BO, the LUMO level of PTB-DCB21 (−3.32 eV) is almost unchanged, but its HOMO level (−5.22 eV) shows a slight increase relative to that of PTB-BO (−5.25 eV). For both polymers, the HOMO energy levels are located above the ground-state level of the perovskite (−5.4 eV),^[1] which indicates that hole transfer from the perovskite to the polymer is expected to occur efficiently.

The hole mobilities of PTB-BO and PTB-DCB21 were measured by the space-charge-limited current (SCLC) method from a hole-only device incorporating PTB-BO and PTB-DCB21, respectively (Figure 3). Hole mobility was determined from Equation (1):

$$J = \frac{9}{8} \epsilon_r \epsilon_0 \mu_h \frac{V^2}{L^3} \quad (1)$$

in which ϵ_0 is the permittivity of free space, ϵ_r is the dielectric constant of the polymers, μ_h is the hole mobility, $V = V_{\text{appl}} - V_{\text{bi}} - V_a$ (V_{appl} is the applied bias, V_{bi} is the built-in potential due to the difference in electrical contact work function, V_a is the voltage drop due to contact resistance and series resistance across the electrodes); and L is the thickness of active layer.^[29,30] The dielectric constant was assumed to be three in our analysis; this is a typical value for conjugated polymers. The hole mobilities of PTB-BO and PTB-DCB21 were measured to be 5.30×10^{-5} and $5.01 \times 10^{-5} \text{ cm}^2 \text{ V}^{-1} \text{ s}^{-1}$, respectively. From UV/Vis absorption, electrochemical redox studies, and hole mobility measurements, the opto-electrochemical properties are not significantly altered by the introduction of the 3,4-dichlorobenzyl group as a side chain of the TT-BDT polymer. The solar cell device was fabricated by using a $\text{CH}_3\text{NH}_3\text{PbI}_3$ absorber, a mesoporous TiO_2 film, and PTB-DCB21 (or PTB-BO) as a HTM. The nanoscopic device structure was verified from cross-sectional field-emission scanning electron microscopy (FE-SEM)

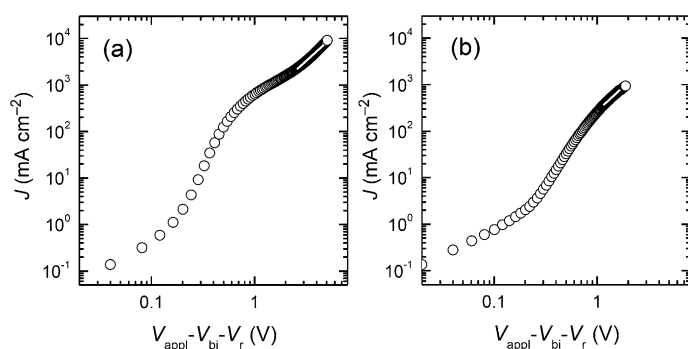


Figure 3. The SCLC (circles) of a hole-only device incorporating the configuration of a) indium tin oxide (ITO)/poly(3,4-ethylenedioxythiophene)-polystyrene sulfonate (PEDOT:PSS)/PTB-BO/Au and b) ITO/PEDOT:PSS/PTB-DCB21/Au. The white line is a linear fit of the data. The current density versus voltage characteristics were recorded on a Keithley 2400 source measure unit.

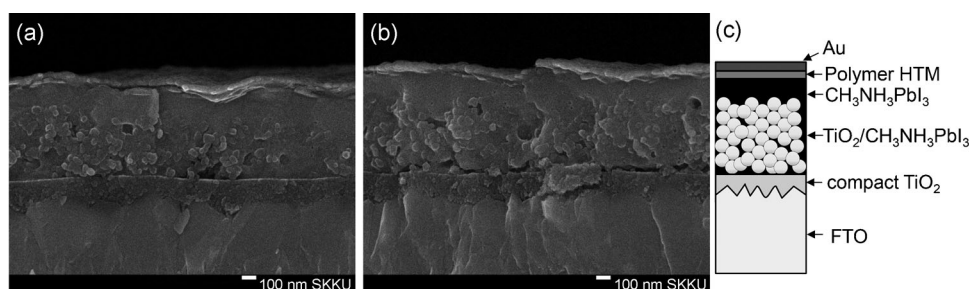


Figure 4. Cross-sectional FE-SEM images of $\text{CH}_3\text{NH}_3\text{PbI}_3$ -based perovskite solar cells employing a) PTB-BO and b) PTB-DCB21. c) Illustration of the layered structure of the perovskite solar cell, showing the infiltrated perovskite in the mesopores of the TiO_2 film. FTO = fluorine-doped tin oxide.

images of the $\text{CH}_3\text{NH}_3\text{PbI}_3$ perovskite solar cell device (Figure 4). The compact nonporous TiO_2 layer forms well on the FTO substrate with a flat surface and its thickness varies from around 130 to 190 nm due to the high haze nature of FTO. The compact TiO_2 layer is necessarily required to prevent direct contact between FTO and HTM. The thickness of the mesoporous TiO_2 film, comprising about 50 nm-sized nanoparticles, is determined to be around 450 nm. Spin-coating of the perovskite precursor solution results in full infiltration of $\text{CH}_3\text{NH}_3\text{PbI}_3$ in the pores and a 120 nm thick capping layer on the mesoporous TiO_2 film. A 50 nm thick polymer layer forms on the perovskite capping layer, which is not well resolved due to overlap with the perovskite layer.

Figure 5 provides a comparison of current density (J) and voltage (V) curves under simulated AM 1.5G one sun illumination and incident photon-to-electron conversion efficiency (IPCE) spectra for the perovskite solar cells employing PTB-DCB21 and PTB-BO. The photovoltaic parameters are summarized in Table 1. The solar cell device containing PTB-DCB21 as a HTM has a J_{sc} of 15.35 mA cm^{-2} , a V_{oc} of 888 mV, and an FF of 0.64, leading to a PCE of 8.7%, whereas the device employing PTB-BO exhibits a lower PCE of 7.4% due to a lower J_{sc} (14.35 mA cm^{-2}) and V_{oc} (827 mV). The IPCE data in Figure 5b are higher over

the entire range of $\lambda = 350\text{--}800 \text{ nm}$ for the PTB-DCB21-bearing device than those for the PTB-BO-containing one. The J_{sc} values (15.49 and 14.38 mA cm^{-2} for PTB-DCB21 and PTB-BO, respectively) calculated by integrating the IPCE data are in good agreement with the directly measured J_{sc} values.

The valley shape of the IPCE spectra at around $\lambda = 670 \text{ nm}$ might be attributed to a loss of reflected light at the gold back contact by polymer HTMs due to absorption of polymer HTMs in this wavelength region, as shown in Figure 1. One observation that supports this hypothesis is that PTB-DCB21 shows an improved IPCE value at $\lambda = 670 \text{ nm}$ relative to that of PTB-BO, in spite of the lower absorption coefficient of PTB-DCB21 ($\approx 34000 \text{ M}^{-1} \text{ cm}^{-1}$ in a solution) than

that of approximately $42000 \text{ M}^{-1} \text{ cm}^{-1}$ for PTB-BO. The photovoltaic performance is remarkable in that the solar cell device does not include any additives, such as lithium bis(trifluoromethanesulfonyl)imide (Li-TFSI) and/or 4-*tert*-butylpyridine (tBP), in the HTM layer: the observed PCEs are much higher than the PCEs of 3–4% recently reported for solar cell devices employing additive-free polymeric HTMs, such as P3HT and poly[N-9-hepta-decanyl-2,7-carbazole-*alt*-3,6-bis(thiophen-5-yl)-2,5-dioctyl-2,5-dihydropyrrolo-[3,4-*b*]pyrrole-1,4-dione] (PCBTDP),^[15,16] Furthermore, compared with the PCE of an additive-free spiro-MeOTAD-based $\text{CH}_3\text{NH}_3\text{PbI}_3$ solar cell, the PTB-DCB21-containing cell has a 24% higher PCE, which is mainly due to the 36.2% higher FF (Figure S3 and Table S1 in the Supporting Information). The effect of lithium salt and tBP additives on the photovoltaic performance of the PTB-DCB21 device is also compared to that of

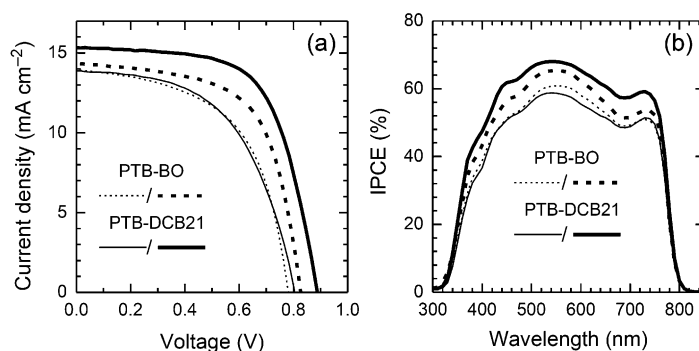


Figure 5. a) J - V curves and b) incident photon-to-electron conversion efficiency (IPCE) spectra of $\text{CH}_3\text{NH}_3\text{PbI}_3$ -based perovskite solar cells employing PTB-BO (dashed lines) and PTB-DCB21 (solid lines) HTMs. J - V curves were obtained under simulated one sun illumination (AM 1.5G, 100 mW cm^{-2}) and the active area of the devices defined by the metal mask was 0.137 cm^2 . Thin and thick lines represent the data for as-fabricated devices and devices aged for 111 h, respectively.

Table 1. Short-circuit photocurrent density (J_{sc}), open-circuit voltage (V_{oc}), fill factor (FF), and PCE of $\text{CH}_3\text{NH}_3\text{PbI}_3$ -based perovskite solar cells employing PTB-DCB21 and PTB-BO HTMs. The performance were measured under simulated one sun illumination (AM 1.5G, 100 mW cm^{-2}) and the active area of the devices defined by a metal mask was 0.137 cm^2 . The data were obtained after aging for 111 h (data in parentheses were obtained from as-fabricated devices).

HTM type	J_{sc} [mA cm^{-2}]	V_{oc} [V]	FF	PCE [%]
PTB-BO	14.35 (13.92)	0.827 (0.781)	0.62 (0.56)	7.4 (6.1)
PTB-DCB21	15.35 (13.89)	0.888 (0.805)	0.64 (0.54)	8.7 (6.0)

the spiro-MeOTAD-based device (Figure S4 and Table S2 in the Supporting Information). The PTB-DCB21-based device shows a slight improvement in PCE by about 9.2% after the addition of additives compared with the large increase in PCE by about 65.7% for the spiro-MeOTAD-based device. This confirms that additive-free PTB-DCB21 is beneficial for the HTM layer in a perovskite solar cell. Upon aging for 111 h, the J - V characteristics for both PTB-BO and PTB-DCB21 devices improved. The device with PTB-DCB21 shows a larger enhancement, as seen in Figure 5 and Table 1, which might be related to the presence of functional groups.

Figure 6 shows a histogram of PCEs for 16 solar cell device samples fabricated under the same conditions. The perovskite solar cells employing PTB-BO show an average PCE of 6.8%, whereas PTB-DCB21 based devices exhibit a mean PCE of about 7.5%. The general trend is that PTB-DCB21-based solar cells generate higher efficiency, by about 10.3%, than those generated by the PTB-BO-based solar cells due to the improved performance in J_{sc} and V_{oc} of the PTB-DCB21 device. Incorporation of the 3,4-dichlorobenzyl group onto the polymer backbone is clearly effective for improving the photovoltaic properties of the $\text{CH}_3\text{NH}_3\text{PbI}_3$ perovskite solar cell. The improved performance is likely to be ascribed to better interactions at the interface between $\text{CH}_3\text{NH}_3\text{PbI}_3$ and PTB-DCB21. The hydrophilic perovskite is expected to make better intermolecular interactions with the relatively polar 3,4-dichlorobenzyl group in PTB-DCB21 rather than the hydrophobic alkyl chains in PTB-BO. Furthermore, the 3,4-dichlorobenzyl group can make various intermolecular interactions with the lead cation of the perovskite, such as cation- π and cation-dipole interactions, because the dichlorobenzyl group has a π system of the benzene ring and a dipole that is induced due to the electronegative chlorine and the electron-donating benzene ring.^[31] The well-constructed polymer HTM-inorganic perovskite heterojunction induced by intermolecular chemical interactions is expected to be beneficial for effective charge separation and transport.

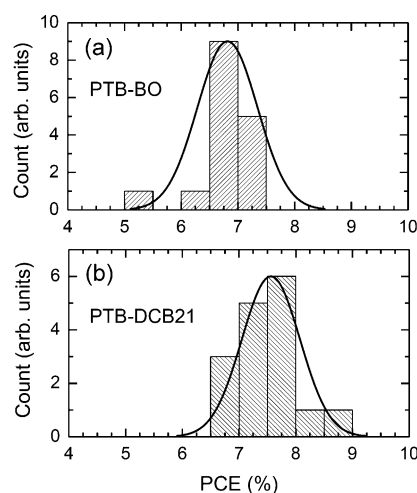


Figure 6. Histogram of PCE for 16 samples of perovskite solar cells employing a) PTB-BO and b) PTB-DCB21 HTMs. The data were obtained from the devices aged for 111 h.

To investigate how functionalization of the HTM polymer with 3,4-dichlorobenzyl groups affects the photovoltaic properties, particularly J_{sc} and V_{oc} , we performed transient photocurrent and voltage spectroscopic studies. The electron diffusion coefficient (D_e) and the time constant for charge recombination (τ_r) were compared (Figure 7). The perovskite solar cell with PTB-DCB21 shows faster electron transport and slower charge recombination than that with PTB-BO. The higher J_{sc} for PTB-DCB21 in comparison with PTB-BO, therefore, results from improved charge collection efficiency due to the higher values of D_e and τ_r . Increased V_{oc} is related to an increase in the Fermi energy level of mesoporous TiO_2 (it may not be excluded that V_{oc} is related to the Fermi level of the perovskite because the perovskite is fully infiltrated in mesoporous TiO_2 with a capping layer) due to slower charge recombination. These results suggest that functionalization of the polymer with 3,4-dichlorobenzyl groups accelerates electron transport and retards charge recombination when compared with the nonfunctionalized polymer. As described in the previous section, intermolecular interactions are expected to make a compact contact between the

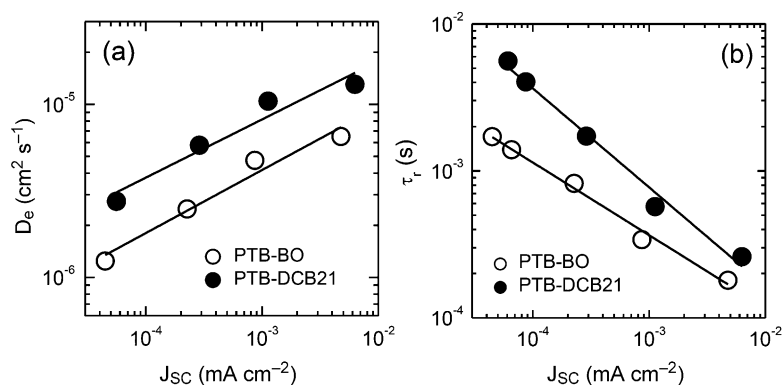


Figure 7. a) Diffusion coefficients and b) time constants for charge recombination as a function of light intensity represented by J_{sc} for perovskite solar cells employing PTB-BO (open circles) and PTB-DCB21 (filled circles) HTMs. The diffusion coefficient was calculated from the time constant for electron transport and TiO_2 film thickness.

polymer and the perovskite, resulting in a well-constructed junction at the molecular level. This can allow effective hole injection from the perovskite layer to the HTM layer by decreasing interfacial transporting resistance and contribute to a reduction in charge recombination at the interface. As a result, the PTB-DCB21-based solar cell device exhibits improved performance in J_{sc} and V_{oc} relative to that of the device containing PTB-BO. The electron diffusion coefficient of about $10^{-5} \text{ cm}^2 \text{ s}^{-1}$ for the present system is similar to those reported on perovskite-sensitized photo-electrochemical solar cells^[7] and the Z907-sensitized solid-state solar cells.^[32] This also indicates that photoexcited electrons in the perovskite are likely to be effectively injected from the perovskite into TiO_2 . Detailed studies are in progress to further understand the charge-transfer/separation dynamics at the interface of the polymer and perovskite layers and the electron diffusion mechanism in the device.

For stability tests of perovskite-based solar cells prepared by using the polymers and aforementioned procedures, the devices were stored in a desiccator without encapsulation before and after J - V measurements. Figure 8 shows changes in the

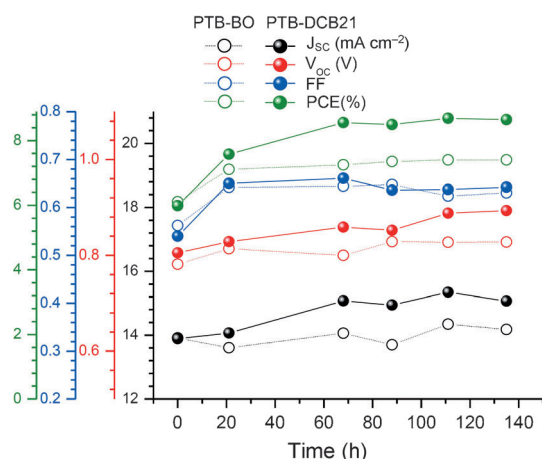


Figure 8. Dependence of J_{sc} , V_{oc} , FF, and PCE on time for perovskite solar cells employing PTB-BO (open circles) and PTB-DCB21 (filled circles) HTMs. The devices were stored in a desiccator at room temperature without encapsulation and measured under simulated one sun illumination (AM 1.5G, 100 mW cm^{-2}).

J_{sc} , V_{oc} , FF, and PCE values in perovskite solar cells employing PTB-DCB21 or PTB-BO as a function of time. The devices do not exhibit any remarkable decrease in solar cell efficiency over 140 h. Interestingly, the PTB-DCB21-containing device shows continuous increases in the PCE for 70 h from 6.0 to 8.7% and remains unchanged thereafter. The efficiency of the PTB-BO-containing device also increases for 20 h from 6.1 to 7.4% and attains a plateau thereafter. The higher PCE value of the PTB-DCB21 device than that of the PTB-BO device upon prolonged aging is attributed to greater changes in both J_{sc} and V_{oc} . Such increases with time are expected to be associated with the presumable change in the HTM-perovskite interface and the larger efficiency increase of 45% for the PTB-DCB21-containing device is probably due to better intermolecular interactions between the perovskite and PTB-DCB21 layers.

3. Conclusions

A new dichlorobenzene-functionalized polymer (PTB-DCB21) was synthesized and used as a HTM for $\text{CH}_3\text{NH}_3\text{PbI}_3$ perovskite solar cells. Compared with the nonfunctionalized polymer (denoted herein as PTB-BO), the perovskite solar cell based on PTB-DCB21 exhibited higher photovoltaic performance with a PCE of 8.7%, owing to higher photocurrent and voltage. Importantly, such a high efficiency was achieved from additive-free PTB-DCB21. The introduction of functionalized PTB-DCB21 was effective in accelerating electron transport and retarding charge recombination in comparison with nonfunctionalized PTB-BO. These improved properties were thought to be correlated to the well-constructed junction at the HTM-perovskite interface through effective intermolecular interactions of $\text{CH}_3\text{NH}_3\text{PbI}_3$ with dichlorobenzene groups. Moreover, the PTB-DCB21-based device showed excellent long-term stability. These preliminary results show that dichlorobenzene functionalization of hole-transporting polymers is a promising way to achieve a high efficiency of perovskite solar cells and deserves to be studied further. Further improvement in the PTB-DCB21-based perovskite solar cell is under study.

Experimental Section

General

Unless stated otherwise, all chemicals were purchased from Aldrich and used without further purification. All of the reactions were performed under an argon atmosphere. Tetrahydrofuran (THF) was distilled over sodium and benzophenone. 4,6-Dibromo-3-fluorothieno[3,4-*b*]thiophene-2-carboxylic acid and 4,8-bis(2-ethylhexyloxy)benzo[1,2-*b*:4,5-*b'*]dithiophene were prepared according to procedures reported in the literature.^[27] ^1H and ^{13}C NMR spectra were recorded at 400 MHz by using a Bruker Ascend 400 spectrometer. Chemical shifts are reported in parts per million (ppm) from low to high frequency and referenced to the residual solvent resonance. Standard abbreviations indicating multiplicity were used as follows: s=singlet, d=doublet, t=triplet, m=multiplet, q=quartet, and br=broad. The molecular weights and distributions of the polymers were determined by GPC with a Jasco Associates liquid chromatography instrument equipped with a PU-2080 pump, an RI-2031 differential refractometer, and a UV-2075 tunable absorbance detector. THF was used as the eluent and polystyrene was used as a standard. The optical absorption spectra were obtained by using a PerkinElmer Lambda 35 UV/Vis spectrometer. Thin films of the polymers were spin-coated from solutions in chlorobenzene, and the film absorption spectra were measured. TGA was conducted on a TA instruments Q50 thermal analysis instrument. DSC was performed on a TA instruments Q20 system.

2'-Butyloctyl-4,6-dibromo-3-fluorothieno[3,4-*b*]thiophene-2-carboxylate (TT-BO)

The prepared materials of 4,6-dibromo-3-fluorothieno[3,4-*b*]thiophene-2-carboxylic acid (1.00 g, 2.77 mmol), *N,N'*-dicyclohexylcarbodiimide (DCC; 687.7 mg, 3.33 mmol), and 4-(dimethylamino)pyridine (4-DMAP; 116.8 mg, 0.96 mmol) were added to a 10 mL round-bottomed flask with CH_2Cl_2 (8 mL). 2-Butyloctanol (2.58 g, 13.85 mmol) was added to the flask and then stirred for 20 h under argon protection. The reaction mixture was poured into

water (100 mL) and extracted with CH_2Cl_2 . The organic phase was dried with anhydrous magnesium sulfate and the solvent was removed. Column chromatography on silica gel with hexane/ CH_2Cl_2 = 4:1 (v/v) as the eluent yielded TT-BO as an oil (806.1 mg, 55.1 %). ^1H NMR (400 MHz, CDCl_3): δ = 0.87–0.93 (m, 6H), 1.26–1.41 (m, 18H), 1.72–1.76 (m, 1H), 4.23 ppm (d, 2H); ^{13}C NMR (100 MHz, CDCl_3): δ = 14.0, 14.1, 22.6, 22.9, 26.7, 28.9, 30.0, 30.9, 31.2, 33.8, 37.3, 68.6, 99.2, 102.0, 119.0, 134.9, 147.3, 150.2, 161.0 ppm.

3',4'-Dichloro-benzyl-4,6-dibromo-3-fluorothieno[3,4-*b*]thiophene-2-carboxylate (TT-DCB)

TT-DCB (236 mg, 32.2 %) was synthesized according to the same procedure as that used for TT-BO from 4,6-dibromo-3-fluorothieno[3,4-*b*]thiophene-2-carboxylic acid (506 mg, 1.41 mmol). ^1H NMR (400 MHz, $\text{C}_2\text{D}_2\text{Cl}_4$): δ = 5.30 (s, 2H), 7.28–7.31 (dd, 1H), 7.50 (d, 1H), 7.54 ppm (d, 1H); ^{13}C NMR (100 MHz, $\text{C}_2\text{D}_2\text{Cl}_4$): δ = 65.7, 99.5, 102.7, 117.4, 127.3, 129.8, 130.7, 132.5, 132.6, 134.5, 135.2, 147.8, 150.7, 160.3 ppm.

2,6-Bis(trimethyltin)-4,8-bis(2-ethylhexyloxy)benzo[1,2-*b*:4,5-*b'*]dithiophene (BDT)

4,8-Bis(2-ethylhexyloxy)benzo[1,2-*b*:4,5-*b'*]dithiophene (4.10 g, 9.18 mmol) was dissolved in anhydrous THF (200 mL) and cooled in an acetone/dry ice bath under argon protection. A solution of butyllithium (2.5 M in hexanes; 8.25 mL, 20.63 mmol) was added dropwise with stirring. The mixture was kept in a dry ice bath for 40 min and then at RT for 20 min. The mixture was cooled in an acetone/dry ice bath and a solution of trimethyltin chloride (27.5 mL, 27.50 mmol; 1 M in THF) was added and stirred at RT overnight. The mixture was quenched with water (50 mL) and extracted with diethyl ether. The organic extract was dried with anhydrous magnesium sulfate and evaporated in vacuo. Recrystallization of the residue from isopropanol yielded BDT (5.24 g, 74.0 %). ^1H NMR (400 MHz, CDCl_3): δ = 0.44 (t, 18H), 0.94 (t, 6H), 1.02 (t, 6H), 1.38–1.73 (m, 16H), 1.78–1.81 (m, 2H), 4.18 (d, 4H), 7.51 ppm (s, 2H); ^{13}C NMR (100 MHz, CDCl_3): δ = –8.2, 11.5, 14.3, 23.3, 24.1, 29.4, 30.7, 40.8, 75.8, 128.1, 133.1, 134.0, 140.5, 143.4 ppm.

PTB-DCB21

2'-Butyloctyl-4,6-dibromo-3-fluorothieno[3,4-*b*]thiophene-2-carboxylate (158.5 mg, 0.30 mmol) and 3,4-dichloro-benzyl-4,6-dibromo-3-fluorothieno[3,4-*b*]thiophene-2-carboxylate (41.5 mg, 0.08 mmol) were weighed into a 10 mL round-bottomed flask. 2,6-Bis(trimethyltin)-4,8-bis(2-ethylhexyloxy)benzo[1,2-*b*:4,5-*b'*]dithiophene (293.5 mg, 0.38 mmol) and $[\text{Pd}(\text{PPh}_3)_4]$ (18.9 mg) were added. The flask was subjected to five successive cycles of vacuum followed by refilling with argon. Then, degassed DMF (1.5 mL) and degassed toluene (6.0 mL) were added by means of a syringe. The reaction was performed at 120 °C for 36 h under argon protection. The raw product was precipitated into methanol and collected by filtration. The polymer was purified by Soxhlet extraction with hexane, methanol, and chloroform. The resulting solid from the chloroform fraction was obtained after drying in vacuo overnight (283.3 mg, 91.9 %). ^1H NMR (400 MHz, CDCl_3): δ = 0.90–2.40 (br, 30H), 3.50–5.40 (br, 6H), 6.50–8.10 ppm (br, 5H); GPC: M_n = 104.9 kg mol $^{-1}$; PDI = 5.48.

PTB-BO

PTB-BO (227.9 mg, 68.7 %) was synthesized according to a similar procedure to that used for PTB-DCB21, with 2'-butyloctyl-4,6-dibromo-

3-fluorothieno[3,4-*b*]thiophene-2-carboxylate (308.9 mg, 0.4 mmol) and 2,6-bis(trimethyltin)-4,8-bis(2-ethylhexyloxy)benzo[1,2-*b*:4,5-*b'*]dithiophene (211.3 mg, 0.4 mmol). ^1H NMR (400 MHz, CDCl_3): δ = 0.70–2.30 (br, 53H), 3.40–5.10 (br, 6H), 6.50–8.00 ppm (br, 2H); GPC: M_n = 112.0 kg mol $^{-1}$; PDI = 2.77.

Electrochemical Studies

CV was performed to investigate the electrochemical properties of the polymers. The polymer thin films coated on a glassy carbon electrode were studied in a 0.1 M solution of Bu_4NPF_6 in acetonitrile at a scan rate of 50 mV s $^{-1}$. Ag/Ag $^+$ was used as a reference electrode. For calibration, the redox potential of ferrocene/ferrocenium (Fc/Fc^+) was measured under the same conditions and located at 0.48 V to the Ag/Ag $^+$ electrode. The redox potential of Fc/Fc^+ is assumed to have an absolute energy level of –4.80 eV to vacuum.^[33] The energy levels of the HOMO and LUMO were then calculated according to Equations (2) and (3), in which ϕ_{ox} is the onset oxidation potential versus Ag/Ag $^+$ and ϕ_{red} is the onset reduction potential versus Ag/Ag $^+$.

$$E_{\text{HOMO}} = -4.8 - (\phi_{\text{ox}} - 0.48) \text{ (eV)} \quad (2)$$

$$E_{\text{LUMO}} = -4.8 - (\phi_{\text{red}} - 0.48) \text{ (eV)} \quad (3)$$

Hole Mobility Measurements

Hole-only devices with a configuration of ITO/PEDOT:PSS/polymer/Au were fabricated. The hole mobilities of the devices were determined by the SCLC method. The dielectric constant was assumed to be three in our analysis; this is a typical value for conjugated polymers. The current density versus voltage characteristics were recorded on a Keithley 2400 source measure unit.

$\text{CH}_3\text{NH}_3\text{I}$

$\text{CH}_3\text{NH}_3\text{I}$ was synthesized as reported elsewhere.^[1,7] Hydroiodic acid (30 mL, 0.227 mol, 57 wt % in water, Aldrich) was placed in a 250 mL round-bottomed flask in an ice bath. To this, a solution of methylamine (27.8 mL, 0.273 mol, 40 wt % in methanol, TCI) was added dropwise by using a syringe, followed by stirring for 2 h. The resulting solution was evaporated at 50 °C for 1 h, which resulted in crystallization of $\text{CH}_3\text{NH}_3\text{I}$. The precipitate was washed three times with diethyl ether and recrystallized from a mixture of ethanol and diethyl ether. Light-yellow $\text{CH}_3\text{NH}_3\text{I}$ was collected on filter paper and dried in vacuum at 60 °C overnight before use. A solution of perovskite $\text{CH}_3\text{NH}_3\text{PbI}_3$ was prepared by mixing (4.8 mmol) $\text{CH}_3\text{NH}_3\text{I}$ (4.8 mmol) and PbI_2 (4.8 mmol; 99 %, Aldrich) in *N,N*-dimethylacetamide (4 mL; 99.8 %, Sigma-Aldrich) at 60 °C overnight.

50 nm-Sized TiO_2

The 50 nm-sized anatase TiO_2 nanoparticles were synthesized by using 20 nm-sized TiO_2 nanoparticles as a seed. The seed TiO_2 nanoparticles were synthesized by autoclaving a hydrolyzed solution of titanium(IV) isopropoxide (97 %, Aldrich) at 230 °C for 12 h.^[34] As synthesized 20 nm TiO_2 nanoparticles were washed three times with deionized (DI) water and dispersed in DI water for use as a seed in a second reaction. In a second reaction, a 0.1 wt % aqueous solution (393.3 mL) containing seed 20 nm TiO_2 and acetic acid (125 mL; >99.7 %, Aldrich) was placed in a 1000 mL round-bottomed flask in an ice bath. Titanium(IV) isopropoxide (60 mL) was mixed with 2-propanol (15 mL), which was added to the seed TiO_2 -

containing solution at a dropping rate of 1.5 mL min^{-1} . After completion of addition, the solution was stirred at 90°C for 6 h, followed by autoclaving at 230°C for 12 h. After cooling to room temperature, TiO_2 nanoparticles were collected by centrifugation and washed with ethanol three times by using an ultrasonicator. TiO_2 paste was prepared by mixing the synthesized TiO_2 particles (ca. 50 nm), terpineol (Aldrich, 99.5%), ethyl cellulose (Aldrich, 46cp), and lauric acid (Fluka, 96%) with a nominal composition of 1.25:6:0.6:0.1. The paste was mixed by using a three-roll-mill for homogeneity before use.

Solar Cell Fabrication

A compact TiO_2 blocking layer was deposited by using 0.15 and 0.3 M solutions of titanium diisopropoxide bis(acetylacetonate) (Aldrich, 75 wt% in isopropanol) in 1-butanol (Aldrich, 99.8%) on FTO glass (Pilkington, TEC-8, $8 \Omega/\text{sq}$). Specifically, the 0.15 M solution was first spin-coated and dried, and then the 0.3 M solution was spin-coated twice. The substrates were dried on a hot plate at 125°C after each coating, and finally annealed at 500°C for 15 min after completion of spinning. A mesoporous TiO_2 layer was deposited on the compact blocking layer by spin-coating precursor solution (200 μL) consisting of TiO_2 paste (2.4 g) and ethanol (10 mL) at 2000 rpm for 20 s, which was followed by annealing at 550°C for 1 h. The annealed mesoporous TiO_2 film was post-treated with TiCl_4 by dipping in a 20 mm aqueous solution of TiCl_4 (Aldrich, >98%) at 70°C for 10 min and then annealing at 500°C for 30 min. Perovskite precursor solution was spun on the resulting mesoporous TiO_2 film at 4000 rpm for 20 s. Perovskite-coated film was dried on a hot plate at 100°C for 15 min. On top of the perovskite capping layer, the polymer HTM layer was deposited by spinning a solution of chlorobenzene (30 μL ; 99.8%, Sigma-Aldrich) including polymer (10 mg mL^{-1}) at 3000 rpm for 30 s. Finally, the counter electrode was formed on the polymer layer by thermal evaporation of Au (ca. 60 nm) at an evaporation rate of 1 \AA s^{-1} .

Photovoltaic Characterizations

Current density and voltage were measured under simulated one sun (AM 1.5G, 100 mW cm^{-2}) by using a solar simulator (Oriol Sol 3A class AAA) equipped with a 450 W xenon lamp (Newport 6279NS) and a Keithley 2400 source meter. The light intensity was adjusted with a NREL-calibrated Si solar cell with a KG-2 filter. The device was covered with an aperture metal mask with an active area of 0.137 cm^2 . The IPCE was measured by a specially designed IPCE system (PV measurement Inc.). A 75 W xenon lamp (USHIO, Japan) was used as a white-light source to generate a monochromatic beam. Transient photocurrent and photovoltage measurements were performed to investigate time constants for transport and recombination of photogenerated electrons by using a transient photocurrent-voltage spectroscopy setup described elsewhere.^[35]

Acknowledgements

This work was supported by National Research Foundation of Korea (NRF) grants funded by the Ministry of Science, ICT & Future Planning (MSIP) of Korea under contract nos. NRF-2010-0014992, NRF-2012M1A2A2671721, NRF-2012M3A7B4049986 (Nano Material Technology Development Program), and NRF-2012M3A6A7054861 (Global Frontier R&D Program on Center for Multiscale Energy System), and the Korea Institute of Science and

Technology (KIST) for "NAP National Agenda Project Program", and project no. 2E23821. J.W.L. is grateful to the NRF for supporting a global Ph.D. grant. We thank Taek-Yong Lee for his assistance in the preparation of 50 nm TiO_2 nanoparticles.

Keywords: electrochemistry • polymers • perovskite phases • semiconductors • solar cells

- [1] H.-S. Kim, C.-R. Lee, J.-H. Im, K.-B. Lee, T. Moehl, A. Marchioro, S.-J. Moon, R. Humphry-Baker, J.-H. Yum, J. E. Moser, M. Grätzel, N.-G. Park, *Sci. Rep.* **2012**, 2, 591.
- [2] J. Burschka, N. Pellet, S.-J. Moon, R. Humphry-Baker, P. Gao, M. K. Nazeeruddin, M. Grätzel, *Nature* **2013**, 499, 316–319.
- [3] M. Liu, M. B. Johnston, H. J. Snaith, *Nature* **2013**, 501, 395–398.
- [4] D. B. Mitzi, C. A. Feild, W. T. A. Harrison, A. M. Guloy, *Nature* **1994**, 369, 467–469.
- [5] K. Chondroudis, D. B. Mitzi, *Chem. Mater.* **1999**, 11, 3028–3030.
- [6] A. Kojima, K. Teshima, Y. Shirai, T. Miyasaka, *J. Am. Chem. Soc.* **2009**, 131, 6050–6051.
- [7] J.-H. Im, C.-R. Lee, J.-W. Lee, S.-W. Park, N.-G. Park, *Nanoscale* **2011**, 3, 4088–4093.
- [8] M. M. Lee, J. Teuscher, T. Miyasaka, T. N. Murakami, H. J. Snaith, *Science* **2012**, 338, 643–647.
- [9] H.-S. Kim, I. Mora-Sero, V. Gonzalez-Pedro, F. Fabregat-Santiago, E. J. Juarez-Perez, N.-G. Park, J. Bisquert, *Nat. Commun.* **2013**, 4, 2242.
- [10] C.-Y. Hsu, Y.-C. Chen, R. Y.-Y. Lin, K.-C. Ho, J. T. Lin, *Phys. Chem. Chem. Phys.* **2012**, 14, 14099–14109.
- [11] S. Holliday, J. E. Donaghey, I. McCulloch, *Chem. Mater.* **2014**, 26, 647–663.
- [12] A. C. Arias, J. D. MacKenzie, I. McCulloch, J. Rivnay, A. Salleo, *Chem. Rev.* **2010**, 110, 3–24.
- [13] J. Zaumseil, H. Sirringhaus, *Chem. Rev.* **2007**, 107, 1296–1323.
- [14] J. H. Heo, S. H. Im, J. H. Noh, T. N. Mandal, C.-S. Lim, J. A. Chang, Y. H. Lee, H.-j. Kim, A. Sarkar, M. K. Nazeeruddin, M. Grätzel, S. I. Seok, *Nat. Photonics* **2013**, 7, 486–491.
- [15] B. Cai, Y. Xing, Z. Yang, W.-H. Zhang, J. Qiu, *Energy Environ. Sci.* **2013**, 6, 1480–1485.
- [16] W. Zhang, R. Zhu, F. Li, Q. Wang, B. Liu, *J. Phys. Chem. C* **2011**, 115, 7038–7043.
- [17] A. Hagfeldt, G. Boschloo, L. Sun, L. Kloo, H. Pettersson, *Chem. Rev.* **2010**, 110, 6595–6663.
- [18] S. Zhang, X. Yang, Y. Numata, L. Han, *Energy Environ. Sci.* **2013**, 6, 1443–1464.
- [19] U. Bach, K. De Cloedt, H. Spreitzer, M. Grätzel, *Adv. Mater.* **2000**, 12, 1060–1063.
- [20] G. Kron, T. Egarter, J. H. Werner, U. Rau, *J. Phys. Chem. B* **2003**, 107, 3556–3564.
- [21] K. Fredin, E. M. J. Johansson, T. Blom, M. Hedlund, S. Plogmaker, H. Siegbahn, K. Leifer, H. Rensmo, *Synth. Met.* **2009**, 159, 166–170.
- [22] H. J. Snaith, M. Grätzel, *Adv. Mater.* **2007**, 19, 3643–3647.
- [23] I. K. Ding, N. Tetreault, J. Brillet, B. E. Hardin, E. H. Smith, S. J. Rosenthal, F. Sauvage, M. Grätzel, M. D. McGehee, *Adv. Funct. Mater.* **2009**, 19, 2431–2436.
- [24] H. J. Son, W. Wang, Y. Liang, L. Li, L. Yu, *J. Am. Chem. Soc.* **2011**, 133, 1885–1894.
- [25] H. J. Son, B. Carsten, I. H. Jung, L. Yu, *Energy Environ. Sci.* **2012**, 5, 8158–8170.
- [26] H. J. Son, L. Lu, W. Chen, T. Xu, T. Zheng, B. Carsten, J. Strzalka, S. B. Darling, L. X. Chen, L. Yu, *Adv. Mater.* **2013**, 25, 838–843.
- [27] Y. Liang, D. Feng, Y. Wu, S.-T. Tsai, G. Li, C. Ray, L. Yu, *J. Am. Chem. Soc.* **2009**, 131, 7792–7799.
- [28] B. Carsten, F. He, H. J. Son, T. Xu, L. Yu, *Chem. Rev.* **2011**, 111, 1493–1528.
- [29] G. G. Malliaras, J. R. Salem, P. J. Brock, C. Scott, *Phys. Rev. B* **1998**, 58, R13411–R13414.
- [30] C. Goh, R. J. Kline, M. D. McGehee, E. N. Kadnikova, J. M. J. Frechet, *Appl. Phys. Lett.* **2005**, 86, 122110–122113.

- [31] E. V. Anslyn, D. A. Dougherty, *Modern Physical Organic Chemistry*, University Science Books, Sausalito, **2006**.
- [32] Y. Zhao, A. M. Nardes, K. Zhu, *J. Phys. Chem. Lett.* **2014**, *5*, 490–494.
- [33] J. Pommerehne, H. Vestweber, W. Guss, R. F. Mahrt, H. Baessler, M. Porsch, J. Daub, *Adv. Mater.* **1995**, *7*, 551–554.
- [34] H.-J. Koo, J. Park, B. Yoo, K. Yoo, K. Kim, N.-G. Park, *Inorg. Chim. Acta* **2008**, *361*, 677–683.
- [35] M.-J. Kim, C.-R. Lee, W.-S. Jeong, J.-H. Im, T. I. Ryu, N.-G. Park, *J. Phys. Chem. C* **2010**, *114*, 19849–19852.

Received: February 14, 2014

Revised: April 10, 2014

Published online on ■ ■ ■, 2014

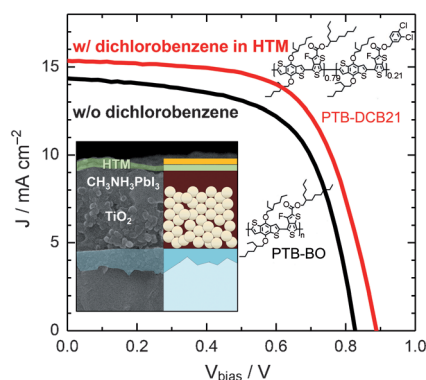
ARTICLES

J.-W. Lee, S. Park, M. J. Ko, H. J. Son,*
N.-G. Park*

■■■ – ■■■



Enhancement of the Photovoltaic Performance of $\text{CH}_3\text{NH}_3\text{PbI}_3$ Perovskite Solar Cells through a Dichlorobenzene-Functionalized Hole-Transporting Material



Made to interact: A functionalized hole-transporting material (HTM) for improved interactions between a halide perovskite and HTM is reported (see picture). A dichlorobenzene-functionalized HTM improves the power conversion efficiency of a $\text{CH}_3\text{NH}_3\text{PbI}_3$ perovskite solar cell by 18.5 %.